Chen *et al.*
*Protection and Control of Modern Power Systems* (2022) 7:15
https://doi.org/10.1186/s41601-022-00237-y

Protection and Control of Modern Power Systems

ORIGINAL RESEARCH Open Access

# A hierarchical coordinated control strategy based on multi-port energy router of urban rail transit

Richeng Chen[1], Yaxi Yang[1] and Tao Jin[1,2*]

**Abstract**

The multi-port energy router (ER) is an effective topology for integrating train traction load, AC load, the energy storage system and photovoltaic(PV) energy. The start and stop process of urban rail transit trains and the access of distributed energy sources to rail transit ER lead to serious fluctuations of DC bus power, so it is necessary to route energy between different ports, involving multi-operating modes, while seamless switching is a major challenge. In this paper, a hierarchical coordinated control strategy is proposed to enable the multi-port ER to operate in a coordinated fashion under the conditions of train parking, acceleration, constant power driving and deceleration, and to switch seamlessly under various working conditions. The energy central dispatching layer sends working condition instructions by sampling the state information of each port, while the microgrid control layer adopts centralized control, receiving upper working condition instructions and sending drive signals to the local control layers to maintain the balanced energy flow of each port. In the local control layers, the PV adopts the improved perturbation and observation method of power control (PC-P&O), while the ES system adopts voltage loop control with an SOC influence factor, voltage loop control with switching factor and power loop control according to the different working conditions, so as to transmit the required train load power accurately and maintain the stability of the DC bus voltage. Finally, the effectiveness of the proposed hierarchical coordination control is verified by MATLAB/Simulink simulations.

**Keywords:** Energy router(ER), Urban rail transit, Hierarchical coordinated control, Seamless switching

## 1 Introduction

Urban rail transit is recognized as a low energy consumption, lower pollution, fast, convenient and safe transportation tool. With the great promotion of Made in China in 2025, it is proposed to build advanced rail transit equipment with technological innovation, high quality and greenness. Therefore, the rail transit industry has become one of the most competitive and innovation-driven fields in China. With the rapid development of urban rail transit, energy saving and intelligence are important development trends [1].

In the urban rail transit system, there is frequent starting, accelerating, braking, etc. In operation, the train traction power fluctuates significantly, which may cause serious security issues to the connected power grid and rail transit network. On the other hand, in order to alleviate human dependence on fossil energy, intermittent and volatile distributed energy generation systems are integrated into the rail transit system network on a large scale [2–4]. It is thus difficult for the power supply network of urban rail transit to withstand large power fluctuations, and consequently an energy router (ER) is introduced to systematically manage energy flow [5].

As the key technology of the energy internet and distributed generation access to the microgrid, an ER has the functions of distribution, transmission and dispatch of electricity [6]. An ER is composed of a series of

*Correspondence: jintly@fzu.edu.cn
[1] College of Electrical Engineering and Automation, Fuzhou University, Fuzhou 350116, China
Full list of author information is available at the end of the article

controlled components, which can be used as the intelligent interfaces of distributed energy, power grid, load and other equipment, so that energy in the network can be reintegrated and managed through the ER. At the same time, connecting a PV system, an energy storage device, train traction load and AC load in rail transit into an ER can realize multi-level distribution and controllable flow of power, better power quality and less power loss [7–10].

With the increasing popularity of renewable distributed generation, a large number of 'energy producers' are rapidly emerging and connected to an ER. For urban rail transit, it is proposed that the PV system connect to the 1500 V DC network of rail transit through DC/DC conversion after analyzing different access methods, in [11]. In view of the rail transit traction power supply system with PV, it is advocated to collect the feedback energy of rail transit braking or excess electricity generated by PV through energy storage devices [12], so as to facilitate the secondary use of electricity and improve power supply efficiency. The battery and supercapacitor are the two main energy storage devices adopted. The introduction of a multi-energy storage system in an ER structure can improve the flexibility of system operation [13], whereas in [14], a self-energy storage system is introduced into the ER to improve the power fluctuation bearing capacity and stabilize the network voltage. In order to quickly respond to power change, a supercapacitor module is introduced in the topology design of a rail transit network in [15, 16]. Through the circuit analysis of the ER, reliable topology structures and control strategies of ER of rail transit are proposed in [17–19].

Under various working conditions of rail transit, using a multi-port ER makes it easy to realize multiple forms of power supply, high reliability, and distributed power plug-and-play access. While energy can be routed in the ER, seamless switching of working conditions is a difficult issue [20, 21]. In [22], the hierarchical and distributed optimization method is adopted to decompose the microgrid dispatching scene into a single microgrid and energy routing sub-problems. This can achieve the seamless connection of energy flow in the dispatching process and improve the dynamic performance of the system. In [23], it is proposed to realize the switching of working conditions based on DC bus voltage signal, but it requires a wide working bus voltage range to ensure the reliable switching of working conditions, and hard switching could cause large voltage fluctuations [24]. A hierarchical and coordinated railway energy management system for an electric traction substation is studied in [25]. The system significantly reduces the cost and energy consumption of train operation. In [26], a HES droop control strategy is proposed to achieve on-grid, off-grid and seamless switching process. A seamless switching method between working conditions is developed in [27], but it only involves the switching between grid-connect and off-grid, and cannot make all converters switch seamlessly. In order to realize the switching of all working conditions, a control strategy based on event response is proposed in [28, 29], but it is still a hard switching, which can cause a large fluctuation of DC bus voltage at the switch instant. To solve the problem [30], it is proposed that the DC bus voltage is controlled by energy storage in the ER to avoid an adverse effect on power quality when working conditions are switched [31]. However, the energy storage capacity needs to be large enough to maintain a small fluctuation of bus voltage during the switching of working conditions.

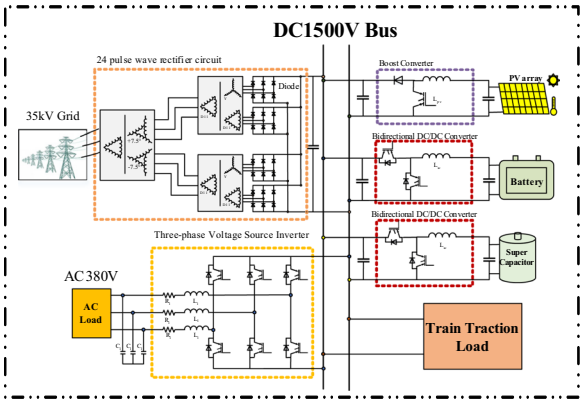


**Fig. 1** Topology of multi-port energy router

Based on the above considerations, a hierarchical coordination control strategy is proposed for the six-port ER of urban rail transit. Given differing working conditions and switching conditions, an improved perturbation and observation method of power control is adopted for PV, while energy storage uses three kinds of control, i.e., voltage loop control with SOC influence factor, voltage loop control with switching factor and power loop control with train power prediction, all to realize the power distribution and transmission for urban rail transit train operation. It shows that the hierarchical coordination control strategy of ER can realize the seamless switching of working conditions and the coordinated operation of multiple working conditions by simulating the switching of different working conditions in the process of a train start and stop process.

## 2 ER topology and hierarchical coordinated control framework

### 2.1 ER topology

The topology of the multi-port ER of urban rail transit proposed in this paper is shown in Fig. 1. The ER ports include: power grid, AC load of train electricity, train

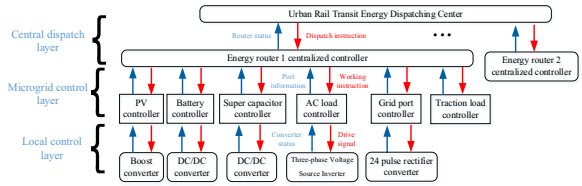


**Fig. 2** Hierarchical coordinated control framework

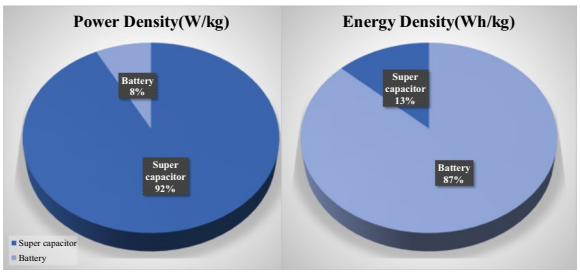


**Fig. 3** Comparison diagram of characteristics of storage battery and super capacitor

traction load, battery, super capacitor and PV ports. The 35 kV power grid is connected to the 1500 V DC bus through the 24-pulse uncontrolled rectifier circuit, and the AC load of the train is connected to the DC bus through the three-phase full-bridge inverter circuit. The PV module is connected to the DC bus through the boost converter, while the battery and supercapacitor energy storage modules are connected to the DC bus through the bidirectional Buck/Boost circuits.

The multi-port ER provides access ports for train traction load, PV, energy storage and the power grid, so that energy in the rail transit power supply network can be flexibly controlled. It is of great importance to ensure the regeneration of train traction energy and to maximize PV energy for the safe and stable operation of the rail transit power supply network under the access of new energy.

### 2.2 Hierarchical coordinated control framework

The hierarchical coordinated control strategy can realize seamless switching between various working conditions. This not only makes full use of distributed energy sources, but also improves the system stability of the rail transit power supply network. The proposed hierarchical coordinated control framework shown in Fig. 2 is divided into three layers according to the priority levels. The first layer is the central dispatching layer with the highest priority, and the centralized controller of the ER responds to the scheduling preferentially according to its own working conditions when there are scheduling instructions. The energy dispatching center of the urban rail transit distributes dispatching instructions to the centralized controller of the ER manually or automatically according to the departure timetable, dispatching situation, traffic status, train operation status, and ER status.

The second layer is the microgrid control layer, and the response priority is secondary to the first layer. When the microgrid control layer receives a scheduling instruction, the working condition instructions are issued to each controller according to the collected port information and ER status. Even if there is no scheduling instruction, the appropriate working condition can be selected based on the current working state of each controller. Among them, PV and energy storage can realize distributed control to a large extent, and only receive switch blocking or opening signals at the moment of access or removal. The third layer is the local control layer with the lowest priority, receiving the drive signal of the microgrid control layer. The local controller controls the switch action of each converter circuit, and uploads the working states of the converters to the microgrid control layer.

The unbalanced energy flowing into the DC bus during transition is fully absorbed by the DC bus capacitor. The fluctuation of bus voltage depends on the unbalanced energy and DC capacitance, as:

$$\begin{aligned} &\left(P_{grid}+P_{pv}+P_{bat}+P_{sc}+P_{train}+P_{load}\right)\\ &\Delta t=0.5C\left(u_{c2}^{2}-u_{c1}^{2}\right) \end{aligned} \tag{1}$$

where $P_{grid}$, $P_{pv}$, $P_{bat}$, $P_{sc}$, $P_{train}$, $P_{load}$ are the power flowing into the DC bus from the 35 kV power grid, PV, battery, super capacitor, train traction load and AC load. $C$ is the equivalent DC bus capacitance, $u_{c1}$ and $u_{c2}$ are the DC bus voltages before and after the working condition is switched, respectively.

The different characteristics of battery and supercapacitor in the energy storage system are shown in Fig. 3. The battery has high energy density but low power density, so the battery capacity is large and can store a large amount of energy. Its instantaneous power flow is small so it is not suitable for instantaneous absorption or release of a large amount of power. However, the supercapacitor has low energy density but high power density, and can instantaneously release or absorb large amounts of power. Therefore, the access of battery and supercapacitor improves the flexibility of the ER.

The microgrid control layer can make the ER perform as an energy router with variable ports, e.g., six-port, ..., two-port, according to the PV output, energy storage state-of-charge (SOC), urban rail transit train operation state (train parking, acceleration, constant power driving, deceleration) and the scheduling instructions of the central dispatching layer. Therefore, a unified coordinated control strategy is needed to realize the safe and stable operation under various working

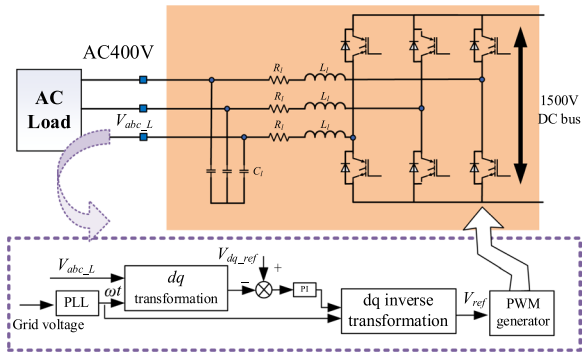


**Fig. 4** DC/AC inverter control strategy diagram

conditions, and realize the seamless switching between different working conditions.

According to the start and stop process of the train, as well as the different working conditions of the light intensity and energy storage SOC, different control strategies are adopted to control the energy storage to provide a large amount of energy during the acceleration phase of the train, and to stabilize the bus voltage. During the deceleration phase of the train, the PV is controlled to reduce its output and the energy storage is controlled to quickly absorb energy and stabilize the bus voltage.

## 3 ER control strategy

### 3.1 Control strategy of three-phase full bridge DC/AC inverter

The circuit realizes bidirectional flow of energy between the AC load and the DC bus, and ensures the power quality of the AC load when the bus voltage fluctuates, so as to realize the safe and stable operation of the electric load on the train. Figure 4 shows the main circuit and control diagrams of the three-phase full-bridge inverter with LC filter. $R_l$ is the equivalent resistance considering various damping factors in the inverter, such as filter inductance internal resistance, dead-time effect, conduction voltage drops of switches and line impedance, $L_l$ is the filter inductance, and $C_l$ is the output filter capacitor.

The three-phase full-bridge inverter circuit adopts the voltage loop control strategy. The voltage of the AC side is measured by voltage sensors, and the phase of the measured AC voltage is then detected by the phase locked loop (PLL) for d-q decomposition. After comparing with the set d- and q-axis voltages, the errors are sent to the PI controllers to generate the dq axis voltage reference $V_{d,q}{}^*$, before transforming back to generate the three-phase reference voltage $V_{\mathrm{ref}}$, which is sent to the PWM generator to generate the control signals for the switches. $V_{d,q}{}^*$ is given as:

$$V_{d,q}^{*} = -\left(K_p + \frac{K_i}{s}\right) * \left(u_{dc\_ref} - u_{dq}\right) \tag{2}$$

where $K_{\mathrm{p}}$ and $K_{\mathrm{i}}$ are parameters of the voltage loop PI controllers. $u_{\mathrm{dq\_ref}}$ and $u_{\mathrm{dq}}$ are the reference voltage of the *dq* axis and the measured *dq* voltage of the AC load, respectively.

### 3.2 Control strategy of energy storage system

The control of the energy storage system is the most critical part of the urban rail transit ER. The energy storage system acts as power source when the train load is high, and stores energy when the train load is low to maintain the stability of the bus voltage. When the train is in urgent need of power support during the acceleration phase, the energy storage quickly releases power, whereas during the deceleration phase of the train the power required drops sharply, and the energy storage quickly absorbs the traction energy and smooths the bus voltage fluctuation.

The energy storage system adopts basic double closed-loop voltage and current control. The voltage loop is formed by comparing the DC voltage with the reference value before feeding into the PI controller, whose output is then compared with the energy storage current and the error is fed into the PI controller in the current loop. An output $V_{\mathrm{ref}}$ is produced and sent to PWM generator to generate switching signals. The control equation can be expressed as:

$$V_{ref} = \left(K_{p2} + \frac{K_{i2}}{s}\right) * \left(\left(K_{p1} + \frac{K_{i1}}{s}\right) * \left(V_{dc\_ref} - V_{dc}\right) - I_{bat}\right) \tag{3}$$

where $K_{\mathrm{p1}}$ and $K_{\mathrm{i2}}$ are PI controller parameters of the voltage loop, whereas $K_{\mathrm{p2}}$, $K_{\mathrm{i2}}$ are PI controller parameters of the current loop. $V_{\mathrm{dc\_ref}}$ and $V_{dc}$ are the reference and measured DC bus voltages, respectively. $I_{\mathrm{bat}}$ is the measured battery output current.

When the SOC of energy storage reaches the limit, the switches controlled by energy storage are blocked. This could result in sudden disappearance of certain energy storage power which will lead to the fluctuation of DC bus voltage. To ensure that the SOC approaches the normal working limit gradually, when the SOC of energy storage is approaching the limit, an SOC influence factor $K_{\mathrm{S}}$ is introduced at the output of voltage loop, so that the power flow of energy storage is reduced in a controlled manner. The energy storage control strategy diagram is shown in Fig. 5, and the expression of $K_{\mathrm{S}}$ is shown in (4) as:

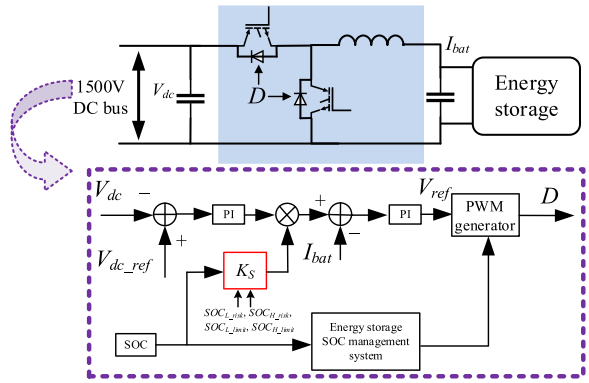


**Fig. 5** Energy storage control strategy diagram under $K_S$ factor

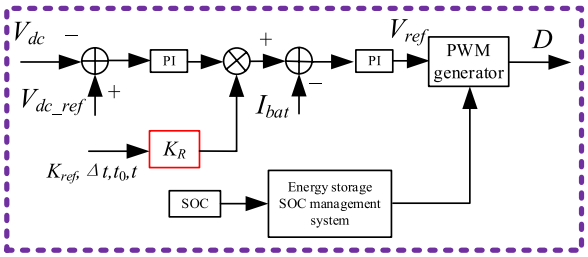


**Fig. 6** Energy storage control strategy diagram under $K_R$ factor

$$K_S = \begin{cases} 1 & SOC_{L\_rick} < SOC < SOC_{H\_rick} \\ \frac{SOC - SOC_{H\_limit}}{SOC_{H\_rick} - SOC_{H\_limit}} & SOC_{H\_rick} \le SOC < SOC_{H\_limit} \\ \frac{SOC - SOC_{L\_limit}}{SOC_{L\_rick} - SOC_{L\_limit}} & SOC_{L\_limit} < SOC \le SOC_{L\_rick} \end{cases} \tag{4}$$

where $SOC_{L\_risk}$ and $SOC_{H\_risk}$ are the upper and lower risk limits of the battery SOC, respectively. $SOC_{L\_limit}$ and $SOC_{H\_limit}$ are the normal operation limits of the battery SOC.

Since the energy storage system in the ER includes a battery and supercapacitor, the coordination between them needs a transition process, as the sudden cut-in or removal of energy storage will cause the fluctuation of bus voltage. When the state is switched, the switching factor $K_R$ is introduced, as shown in Fig. 6 and given as:

$$K_R = \begin{cases} K_{ref} * \frac{t - t_0}{\Delta t} & t - t_0 \le \Delta t \\ K_{ref} & t - t_0 > \Delta t \end{cases} \tag{5}$$

where $K_{ref}$ is the set PI controller gain, $t_0$ and $t$ are the state switching time and current time, respectively. $\Delta t$ is the set switching time interval.

Th supercapacitor can provide large power in a short period, and so can provide for the power demand when the train is accelerated. However, the PI control of the voltage loop has hysteresis, which cannot fully exploit the advantages of the supercapacitor. Therefore, the power loop control is adopted for peak cutting and valley filling of train, as shown in Fig. 7. The supercapacitor adopts power control to collect the power of the train through the microgrid control layer, and then divides by the voltage of the supercapacitor to obtain the reference current, which is compared with the measured current before feeding to the PI controller. Finally, the generated $V_{ref}$ is sent to the PWM generator to control the switches and the control equation can be expressed as:

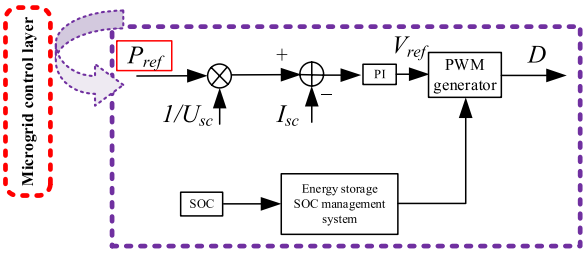


**Fig. 7** Energy storage power loop control strategy diagram

$$V_{ref} = \left(K_{p3} + \frac{K_{i3}}{s}\right) * \left(\frac{P_{ref}}{U_{sc}} - I_{sc}\right) \tag{6}$$

where $K_{p3}$ and $K_{i3}$ are the PI controller parameters of the current loop, $U_{sc}$ is the voltage of the supercapacitor, $P_{ref}$ is the train power collected by microgrid control layer, and $I_{sc}$ is the measured output current of the supercapacitor.

### 3.3 Control strategy of PV system

Traditional PV control adopts maximum power point tracking (MPPT), which can output the maximum power according to the light intensity and temperature, but the power cannot be controlled actively.

When light is sufficient and the SOC of energy storage is high, there is surplus energy in the ER, so it is desirable to limit the PV output power to ensure that energy storage is in the normal working state. Therefore, an improved perturbation and observation method for power control (PC-P&O) is proposed. The PV control block diagram is shown in Fig. 8, and the control strategy can switch between the normal P&O MPPT strategy and the PC-P&O control strategy according to different working conditions.

When the local control layer receives the instruction of limiting PV power to $P_{ref}$ from the microgrid control layer, PV rapidly reduces the output power to $P_{ref}$ through PC-P&O. When the PV output power decreases, the change of duty ratio is consistent with the previous one, while the operation is contrary to the previous one when the PV output power increases. At

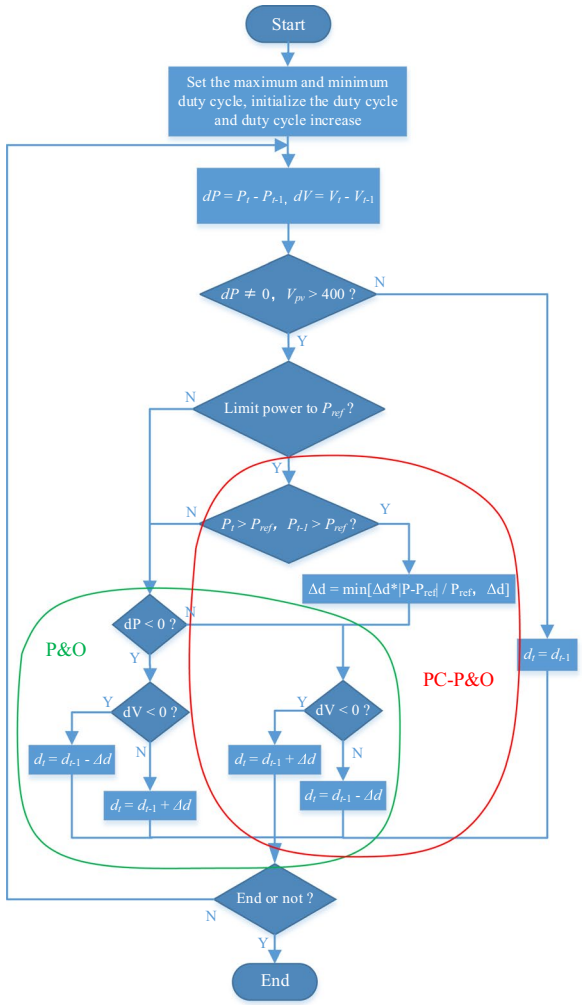


**Fig. 8** PC-P&O control block diagram

the same time, when the difference between PV output power and $P_{ref}$ is large, the duty ratio step $\Delta d$ will also increase to ensure that the reference power point can be reached quickly.

When the train is decelerating, the traction power flows back to the DC bus. In order to ensure the stability of the bus voltage and release the pressure of energy storage from absorbing energy, the PV is controlled by PC-P&O to reduce its output to further ensure the stability of the bus voltage.

### 3.4 Effectiveness evaluation index of control strategy

Switching between different working conditions will inevitably lead to fluctuation of the DC bus voltage. In order to reduce the fluctuation, a coordinated control strategy is adopted to realize seamless switching between working conditions and stabilize the bus

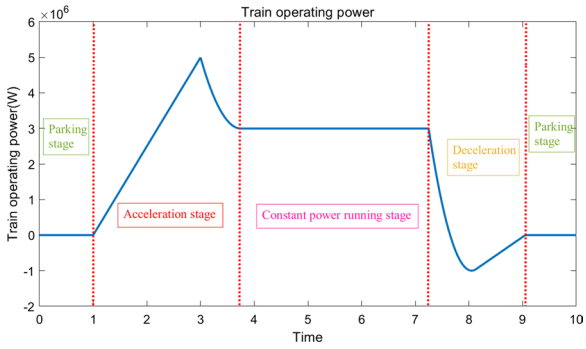


**Fig. 9** Diagram of train power variation

voltage. The voltage fluctuation index $V_{ol\_volatility}$ is defined as:

$$V_{ol\_volatility} = \frac{\sum_{i=k}^{n} |V_{dc\_i} - V_{dc\_ref}|}{V_{dc\_ref} * (n-k)} * 100\% \quad (7)$$

where $k$ and $n$ are the starting and ending voltage sampling points of the switching process, $V_{dc\_i}$ is the i$^{th}$ DC bus sampling voltage, and $V_{dc\_ref}$ is the reference DC voltage. It should be noted that the voltage fluctuation index needs to be maintained within 3% to ensure the safe and stable operation of the whole system.

## 4 Design and switching of working conditions

### 4.1 Design of traction load power and PV output

The change trend of train power during start and stop is shown in Fig. 9. As seen, the traction power of the train is 0 during the stop stage, and rises rapidly when the train starts to accelerate. When the speed of the train reaches a certain value, the traction power decreases, and then maintains a constant power. During the braking stage, the traction power decreases rapidly, and after it drops to zero, the traction power releases a period of energy to the 1500 V DC bus before recovering to zero again when the train stops. In this simulation, the traction power is set to 3 MW when the train runs at constant power, the maximum traction power can reach 5 MW during the acceleration stage, and the minimum power is -1 MW during the deceleration stage.

Figure 10 shows the maximum output power diagram of PV controlled by the MPPT algorithm under certain setting light intensity and temperature fluctuations. By simulating the changes of light intensity and temperature in different periods, the output power of the PV system is changed.

### 4.2 Parking condition

The port state and control mode of the parking condition are shown in Table 1. For the grid, C represents grid

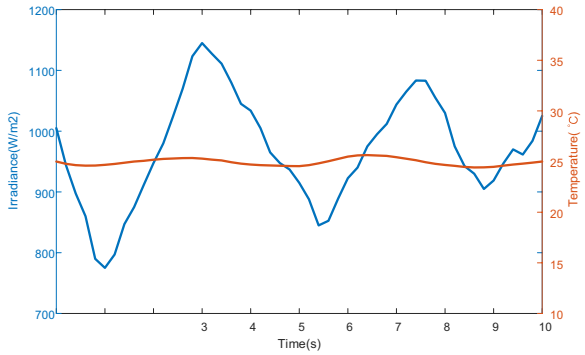


**Fig. 10** Working condition design of PV system

connection and D represents grid disconnection. For the energy storage control strategy, VC represents voltage loop control, PC represents power loop control, whereas for energy storage status, $SOC_{Bat}$, $SOC_{SC}$ and $SOC_{ES}$ represent the state of charges of the battery, supercapacitor, and energy storage system, respectively.

During train parking, six basic conditions (C1.1–C1.6) are divided according to the SOC of energy storage and PV energy during day and night, as listed in Table 1.

(1) When PV energy is sufficient while the SOC of energy storage is less than 60%, PV adopts the P&O MPPT algorithm, energy storage adopts the voltage and current double closed-loop control, and the power grid is connected to the ER through the 24-pulse uncontrolled rectifier circuit, as in C1.1. When the SOC of energy storage is in the range of 60–80%, the power grid is disconnected, and the energy storage is charged by PV, as in C1.2. When the SOC of energy storage is in the range of 80–90%, which is approaching the upper limit, the control strategy of PV is switched to PS-P&O to reduce its output power to charge the energy storage slowly, as in C1.3. When the SOC of energy storage is higher than 90%, the PV and energy storage ports are disconnected, as in C1.4.

(2) When the PV energy is insufficient at night, PV is disconnected, and the energy storage is charged by the grid, as in C1.5. When the SOC of energy storage is higher than 90%, the grid and energy storage are disconnected, as in C1.6.

**Table 1** Port state of the stop state and the control mode

| Case | Status | | Control mode | | |
|---|---|---|---|---|---|
| | PV | $SOC_{Bat}$ | PV | Bat | Grid |
| Day | | | | | |
| C1.1 | Adequate | < 60% | P&O | VC | C |
| C1.2 | Adequate | 60–80% | P&O | VC | D |
| C1.3 | Adequate | 80–90% | PS- P&O | VC | D |
| C1.4 | Adequate | > 90% | D | D | D |
| Night | | | | | |
| C1.5 | Deficient | ≤ 90% | D | VC | C |
| C1.6 | Deficient | > 90% | D | D | D |

**Table 2** Port state and control mode for acceleration condition

| Case | Status | | Control mode | | |
|---|---|---|---|---|---|
| | PV | $P_{train}$ | PV | Bat | SC |
| Day | | | | | |
| C2.1 | Adequate | $\leq P_{cp}$ | P&O | VC | D |
| C2.2 | Adequate | $> P_{cp}$ | P&O | VC | PC |
| Night | | | | | |
| C2.3 | Deficient | $\leq P_{cp}$ | D | VC | D |
| C2.4 | Deficient | $> P_{cp}$ | D | VC | PC |

### 4.3 Accelerating condition

The port states and control modes of the accelerating condition are shown in Table 2. When the train is accelerating, the grid port is always connected. Since the energy storage system is charged under the parking condition, the energy storage SOC is usually in full state when accelerating, so an insufficient SOC of energy storage is not considered in this condition. The accelerating condition is divided into four basic conditions (C2.1-C2.4) according to the PV energy and the accelerating power.

(1) When the PV energy is sufficient, PV adopts P&O MPPT algorithm, the battery adopts the voltage and current double closed-loop control, and grid is connected. If the train power ($P_{train}$) is lower than the value when the train runs at constant power($P_{cp}$), the supercapacitor is disconnected. In the contrary state, the supercapacitor adopts power loop control, so the required power higher than $P_{cp}$ in the train accelerating stage is provided by the rapid release of power from the supercapacitor.

(2) When the PV energy is insufficient at night, PV is disconnected, and the control modes of the other ports are consistent with those when the PV energy is sufficient.

### 4.4 Constant power condition

The port states and control modes of the train running at constant power condition are shown in Table 3. In such a condition, the grid is always connected, and it is divided into six basic working conditions (C3.1–C3.6) according to PV energy and the SOC of energy storage.

(1) When the PV energy is sufficient, PV adopts the P&O MPPT algorithm and the grid is connected. When the SOC of the battery is higher than 30%, the voltage and current double closed-loop control is adopted, while the supercapacitor is disconnected.

**Table 3** Port state and control mode under constant power running condition

| Case | Status | | Control mode | | |
|---|---|---|---|---|---|
| | PV | $SOC_{ES}$ | PV | Bat | SC |
| Day | | | | | |
| C3.1 | Adequate | $SOC_{Bat} > 30\%$ | P&O | VC | D |
| C3.2 | Adequate | $SOC_{Bat}$:20–30% $SOC_{SC}: \geq 20\%$ | P&O | VC | VC |
| C3.3 | Adequate | $SOC_{Bat}$:20–30% $SOC_{SC}: < 20\%$ | P&O | VC | D |
| C3.4 | Adequate | $SOC_{ES:} < 20\%$ | P&O | D | D |
| Night | | | | | |
| C3.5 | Deficient | $SOC_{Bat:} > 30\%$ | D | VC | D |
| C3.6 | Deficient | $SOC_{Bat}$:20–30% $SOC_{SC}: \geq 20\%$ | D | VC | VC |

**Table 4** Port state and control mode of deceleration condition

| Case | Status | | Control mode | | |
|---|---|---|---|---|---|
| | PV | $SOC_{Sc}$ | PV | Sc | Grid |
| Day | | | | | |
| C4.1 | Adequate | < 80% | PC-P&O | VC | D |
| C4.2 | Adequate | 80–90% | PC-P&O | VC | D |
| C4.3 | Adequate | > 90% | PC-P&O | D | D |
| Night | | | | | |
| C4.4 | Deficient | < 90% | D | VC | D |
| C4.5 | Deficient | > 90% | D | D | D |

When the SOC of battery is in the range of 20–30%, the supercapacitor is connected to the ER by the VC control strategy if the supercapacitor SOC is higher than 20%, and if the SOCs of battery and supercapacitor are both lower than 20%, the storage system is disconnected.

(2) When the PV energy is insufficient at night, PV is disconnected, and the control modes of the other ports are consistent with those when PV energy is sufficient.

### 4.5 Decelerating condition

The port states and control modes of decelerating condition are shown in Table 4. In such a condition, the power grid is always connected, and the battery always adopts voltage and current double closed-loop control. The working condition is divided into five basic conditions (C4.1–C4.5) according to the PV energy and the SOC of energy storage.

(1) When the PV energy is sufficient and the SOC of the supercapacitor is less than 80%, PV adopts the MPPT algorithm, while the supercapacitor adopts voltage and current double closed-loop control. When the SOC of the supercapacitor is between 80 and 90%, PV adopts PS-P&O control, and when the supercapacitor SOC is above 90%, it is disconnected.

(2) When the PV energy is insufficient at night, PV is disconnected. If the super capacitor SOC is less than 90%, it adopts voltage and current double closed-loop control, otherwise it is disconnected.

### 4.6 Design of working condition switching

(a) Switching of energy storage control

When the energy storage is connected to or disconnected from the ER, the voltage and current double closed-loop control with influence factor KR is adopted. Through KR, the impact of cut-in or cut-off of energy storage on bus voltage can be greatly reduced, such as from C2.1 to C3.2, C3.1 to C3.2, and C3.1 to C4.1

Whenever the energy storage is removed from the ER because SOC is about to exceed the working range, such as from C1.3 to C1.4, C3.2 to C3.3, C4.2 to C4.3, the impact on the ER can be alleviated by using the voltage and current double closed-loop control with SOC influence factor $K_S$, which greatly reduces the impact of switching working conditions on DC bus voltage.

During working conditions from C2.1 to C2.2, and C2.3 to C2.4, when the train is under acceleration and the traction power is larger than the value when running at constant power, the supercapacitor changes from the standby state to the power control state to quickly provide the additional train traction power exceeding $P_{cp}$.

(b) Switching of PV control

When the PV energy is sufficient, and the SOC of energy storage is about to reach the upper limit or the train is in a state of deceleration, the PS-P&O control is adopted to alleviate the energy absorption rate to protect the service life of energy storage or suppress the excessive increase of bus voltage caused by train deceleration. For example, the working conditions from C1.3 to C1.4, and C4.1 to C4.2, can achieve the purpose of alleviating the bus voltage fluctuation.

## 5 Simulation and analysis of working conditions

In order to verify the effectiveness of the proposed coordinated control strategy, the existing control strategy is simulated and analyzed first, and then the control strategy proposed in this paper is simulated and analyzed under typical operating conditions.

### 5.1 Existing control strategy

The traditional rail transit energy router control strategy does not distinguish between different working conditions. During the start and stop of the train, the energy storage adopts double closed-loop voltage stabilization control, and the PV adopts P&O control strategy. The simulation results are shown in Fig. 11. It can be seen that the traditional control strategy has a great impact on the bus voltage fluctuation during the start and stop of the train, especially in the acceleration and deceleration phases, i.e., the DC bus voltage fluctuates more than 2% during acceleration and over 20% during deceleration. It can be seen that the traditional energy router control method is not suitable for rail transit application.

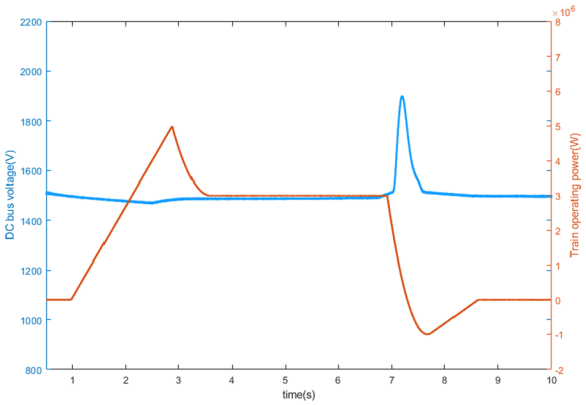


**Fig. 11** Simulation waveform diagram of the traditional rail transit energy router control strategy

### 5.2 Switching of typical working conditions in train parking

The proposed control strategy is adopted and Fig. 12 shows the simulated results for switching between typical working conditions when the train is stopped. As seen, before 3.1 s, the ER is in the working condition C1.1. The SOC of battery is lower than 60%, the grid is connected, PV works in the MPPT state, and the battery is charged by voltage loop control. The SOC of the supercapacitor is less than 80% before 1 s and is charged by voltage loop control. After 1 s, the SOC is about to reach the limit and the voltage loop control with SOC influence factor $K_S$ is adopted. With the SOC oft the supercapacitor close to 90%, the charging power is reduced gradually, as shown in Fig. 12.

During 3.1–8.5 s, the ER is in working condition C1.2, the battery SOC is between 60 and 80%, the power grid is disconnected, and PV is still working in the MPPT state. The battery is charged by voltage loop control, and the supercapacitor is disconnected because of reaching the charging upper limit. At 8.5 s, the battery SOC is higher than 80% and the working condition is switched to C1.3. After 8.5 s, the grid is still disconnected, the battery adopts the voltage loop control with SOC influence factor $K_S$, and PV adopts the PS-P&O control to limit output power, to ensure slow charging of battery to prolong its life. It can be seen that the DC bus voltage fluctuation is less than 0.8% in the switching process of typical working conditions under train parking. This not only improves the service life of energy storage devices, but also realizes seamless switching of working conditions. From the results, the effectiveness of the proposed control strategy is fully verified.

### 5.3 Switching of typical working conditions in train acceleration

In the working condition of C1.2 before 4 s, the train is in the parking state, the battery SOC is larger than 60% and is charged by voltage loop control, PV is in the MPPT state, while the power grid and supercapacitor are both disconnected, as shown in Fig. 13.

The train starts to accelerate between 4 and 5.2 s. The working condition is thus switched to C2.1 while traction power is lower than $P_{cp}$ and the power grid is connected to the ER. The working condition is switched to C2.2 between 5.2 and 6.8 s, during which time traction power exceeds $P_{cp}$. The supercapacitor is switched from standby state to power loop control to provide the required traction power exceeding $P_{cp}$. The working condition becomes C3.1 after 6.8 s, the train runs under constant power and the supercapacitor is disconnected. Similarly, the fluctuation of the DC bus voltage is lower than 1.2% during the whole process of acceleration. The proposed hierarchical coordinated control strategy enables the supercapacitor to realize accurate power distribution according to the instructions of microgrid control layer during acceleration, while it also maintains the stability of DC bus voltage and realizes the seamless switching of working conditions.

### 5.4 Switching of typical working conditions in constant power state

During the period of 0.5–3.2 s, the train is in an accelerated state, and the working conditions change from C2.1 to C2.2. The grid is connected, the battery adopts voltage loop control, and PV works in the MPPT state, as shown in Fig. 14.

At 3.2 s, the train is in the constant power driving state and the working condition is changed from C2.2 to C3.1. The power grid, battery and PV do not change during working state switching, while the supercapacitor switches from power loop control to standby state. At 9 s, the SOC is reduced to 30% because of the continuous discharge of the battery during constant power

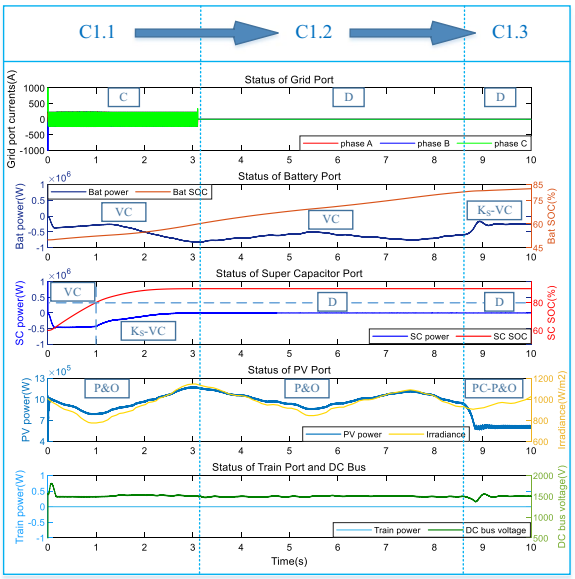


**Fig. 12** Simulation waveform diagram of each port for switching between typical working conditions when the train is stopped

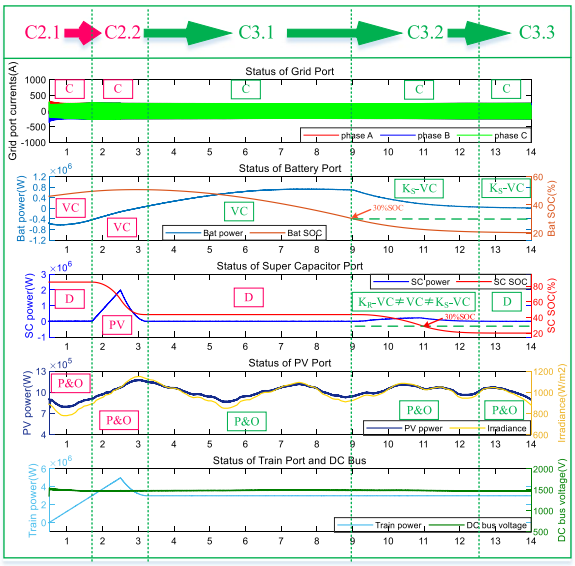


**Fig. 14** Simulation waveform diagram of each port of the typical working condition switching under the constant power of the train

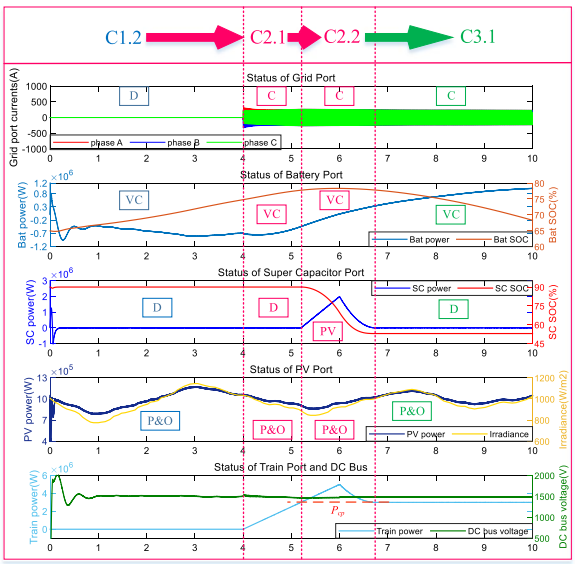


**Fig. 13** Simulation waveform diagram of each port of the typical working condition switching under the acceleration state of the train

driving, and the working condition is C3.2. The battery control mode is changed to voltage loop control with the SOC influence factor $K_S$. At this time, the supercapacitor is connected to the ER, and the voltage loop control with influence factor $K_R$ is switched to the normal voltage loop control after 0.5 s. When the supercapacitor SOC is less than 30% at 11 s, it is switched to voltage loop control with SOC influence factor $K_S$. The SOC of the supercapacitor reaches the lower limit of 20% at 12.5 s, the working condition is switched to C3.3 and the supercapacitor is disconnected. During the switching process of typical working conditions under constant power driving, the fluctuation of DC bus voltage is less than 1.3%, which indicates seamless switching of working conditions and verifies the effectiveness of the proposed hierarchical coordinated control strategy.

### 5.5 Switching of typical working conditions in train deceleration

During the period of 3.5–6.8 s, the working condition is C3.1 and the train runs at constant power. The grid is connected, the battery adopts voltage loop control, PV works in MPPT state, and the supercapacitor is disconnected, as shown in Fig. 15.

At 6.8 s, the train is decelerating, and the working condition is switched from C3.1 to C4.1. The supercapacitor is connected to the ER, and the voltage loop control with influence factor KR is switched to normal voltage loop control after 0.5 s. During the whole deceleration period, the PC-P&O control strategy is adopted to reduce serious fluctuation of the bus voltage when the train regenerates energy. At 8.8 s, the train is in the parking state and the working condition is switched to C1.1, because the SOC of the battery is less than 60% and PV adopts the normal MPPT control. During the whole decelerating process, the DC bus voltage remains steady during the switching of various typical working conditions, and the bus voltage fluctuation index is only 1.6%. The results fully verify that the proposed

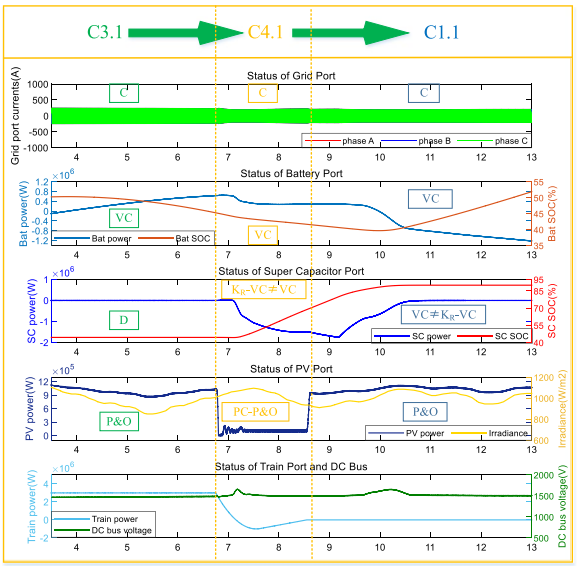


**Fig. 15** Simulation waveform diagram of each port of typical working condition switching under train deceleration state

hierarchical coordinated control strategy can integrate the seamless switching of various working conditions.

## 6 Conclusion

Based on the topology of six-port ER for urban rail transit, this paper proposes a hierarchical coordination control strategy for multi-condition coordinated operation and seamless switching of an ER. According to the different working conditions, voltage loop control with SOC influence factor $K_S$, switching factor $K_R$ and power loop control are adopted, so that the exchanged power of energy storage can be accurately controlled and coordinated, to ensure the service life of energy storage and stabilize the DC bus voltage. PV adopts the PC-P&O control strategy to ensure that its power is controlled and reduced when there is excessive energy. The effectiveness of the proposed hierarchical coordinated control strategy is verified by MATLAB simulations, in which the ER is coordinated in operation under various typical working conditions of urban rail transit trains, and the indices of the DC bus voltage meet requirements.

**Acknowledgements**
This work was primarily supported by the Chinese National Natural Science Foundation (grant number 51977039 and 51950410593).

**Authors information**
Richeng Chen was born in Fujian province, China, in 1997. He received bachelor degree (2019) from College of Electrical Engineering & Automation, Fuzhou University. Since 2019, He is working toward the master degree in the Department of Electrical Engineering and Automation of Fuzhou University. His current research interests include control strategy of urban rail energy router and dynamic detection of track performance.
Yaxi Yang was born in Jiangxi province, China, in 1998. She received bachelor degree (2019) in Electrical Engineering and Automation from Fuzhou University. Since 2019, She is working toward the master degree in the Department of Electrical Engineering and Automation of Fuzhou University. Her current research interests include track irregular detection, VSG control and urban track traffic.
Tao Jin (SM'2019) received B.S. and M.S. degrees in Electrical Engineering from Yanshan University respectively in 1998 and 2001, and the Ph.D. degree in Electrical Engineering from Shanghai Jiaotong University in 2005. From 2005 to 2007, he worked as a postdoctor in Shanghai Jiaotong University. During this time, he was in charge of a research group in the biggest dry-type transformer company in Asia, Sunten Electrical Co.Ltd, to develop new transformer technology with distribution grid. From 2008 to 2009, he held research scientist position with Virginia Tech, Blacksburg, USA, where he was involved in the design and test of PMU technology and GPS/internet-based power system frequency monitoring network. In 2010, he joined Imperial College London, UK, as European Union Marie Curie Research Fellow, where he was focused on electrical technologies related to smart grid. Now he is a professor in College of Electrical Engineering & Automation, Fuzhou University, China. Prof. Tao Jin has published about 150 papers, and he is members of IEEE Power and Energy Society and IEEE Industrial Electronics Society, and special committee members of Chinese Society of Electrical Engineering, China Electrotechnical Society, and etc. He currently serves as associate editors for MPCE, PCMP, China Measurement & Testing Technology, and other journals.

**Authors' contributions**
All authors contributed to the study conception and commented on previous versions of the manuscript. RC completed the design and Simulation of train working conditions in the paper and the compilation of the paper. YY was mainly responsible for the selection of circuit parameters in the energy router and put forward modification suggestions for the language of the paper. TJ guided the direction of the paper and put forward modification suggestions. All authors read and approved the final manuscript.

**Funding**
This work was primarily supported by the Chinese National Natural Science Foundation (Grant Numbers 51977039 and 51950410593).

**Availability of data and materials**
Please contact author for data and material request.

## Declarations

**Competing interests**
The authors declare that they have no known competing financial interests or personal relationships that could have appeared to influence the work reported in this paper.

**Author details**
[1]College of Electrical Engineering and Automation, Fuzhou University, Fuzhou 350116, China. [2]Fujian Key Laboratory of New Energy Generation and Power Conversion, Fuzhou 350116, China.

Received: 5 June 2021 Accepted: 26 March 2022
Published online: 13 April 2022

**References**

1. Chunhua, Y., Hairong, D., & Yisheng, Lv. (2019). Preface to the special issue on intelligent rail transit system. *Acta Automatica Sinica, 45*(12), 2205–2207.
2. Guorong, Z., & Xiaran, C. (2017). Future development of energy internet. *Electric Power Automation Equipment, 37*(1), 1–7.
3. Yu, H., Li, G., Yang, B., & Zhu, S. (2021). Research on the active control technology of grid voltage based on a distributed photovoltaic/flywheel energy storage combined generation system. *Power System Protection and Control, 49*(3), 48–56.
4. Chen, Z., Zhang, X., Wang, X., et al. (2021). A distributionally robust optimal allocation method for distributed photovoltaic generation stations integrated into a distribution network. *Power System Protection and Control, 49*(13), 30–42.

5. Hui, G., Fei, W., Lijun, Z., & Jian, L. (2016). Intelligent distributed energy network technology based on energy router. *Proceedings of The Chinese Society for Electrical Engineering, 36*(12), 3314–3325.
6. Roasto, I., Husev, O., Najafzadeh, M., & Jalakas, T. (2019). Voltage source operation of the energy-router based on model predictive control. *Energies, 12*(10), 1892–1906.
7. Gaohui, F., Zhengming, Z., & Liqiang, Y. (2017). Integrated control technology of power router based on energy balance. *Transactions of China Electrotechnical Society, 32*(14), 34–44.
8. Wanxing, S., Penghua, L., Qing, D., Zhen, L., & Cunhao, Z. (2019). Research on energy management strategy of energy hub based on Lyapunov optimization method. *Proceedings of The Chinese Society for Electrical Engineering, 39*(21), 6212–6225.
9. Takahashi, R., Kitamori, Y., & Hikihara, T. (2013). Ac power local network with multiple power routers. *Energies, 6*(12), 6293–6303.
10. Murty, V. V. S. N. (2020). Ashwani Kumar, "Multi-objective energy management in microgrids with hybrid energy sources and battery energy storage systems." *Protection and Control of Modern Power Systems, 5*(4), 304–310.
11. Weirong, C., Xuan, W., Qi, Li., Ying, H., & Weiying, W. (2019). Review on the development of traction power supply system for photovoltaic power station connected to rail transit. *Power System Technology, 43*(10), 3663–3670.
12. Wenli, D., Zhao-Hua, D., & Wei-Rong, C. (2019). Application of photovoltaic in ac/dc traction power supply system under the background of rail transit energy Internet and analysis of key problems. *Proceedings of The Chinese Society for Electrical Engineering, 39*(19), 5692–5702.
13. Arun Kumar, V., Sumedha, S., & Ashu, V. (2019). Optimal sizing and multi-energy management strategy for PV-biofuel-based off-grid systems. *IET Smart Grid, 3*(1), 83–97.
14. Sheng, W., Lan, Z., Duan, Q., Li, Y., Ma, C., & Lv, Z. (2014). Research on self-storage energy router. *Power System Technology, 41*(2), 387–393.
15. Kuan, C., & DianboGuansheng, R. F. (2014). Research and development summary of supercapacitor used in rail transit. *Battery Bimonthly, 44*(5), 296–298.
16. Huaixin, C., Zhongping, Y., Fei, L., Huan, X., Bin, W., & Kunyu, W. (2019). Management and configuration for stationary super-capacitor energy storage system applied in urban rail transit based on genetic algorithm. *Journal of the China Railway Society, 41*(9), 59–66.
17. Xin, A., Jingguo, R., Zheng, L., Yunning, L., & Kunyu, W. (2019). Research on a new energy router structure and its control strategy. *Power System Technology, 43*(4), 1202–1210.
18. Yang, C., Liqiang, Y., Shaomin, Z., Renle, H., Gao-Hui, F., & Zheng-Ming, Z. (2015). Design of key parameters of power distribution network energy router for energy Internet. *Power System Technology, 39*(11), 3094–3101.
19. Kai, L., Caixue, C., Jun, W., Houda, Z., & Kai, L. (2018). Energy router based on hierarchical coordinated control of energy. *Acta Energiae Solaris Sinica, 39*(5), 1388–1395.
20. Liu, B., Peng, Y., Xu, J., Mao, C., Wang, D., & Duan, Q. (2021). Design and implementation of multiport energy routers toward future energy Internet. *IEEE Transactions on Industry Applications, 57*(3), 1945–1957.
21. Li, S., Wu, C., Xiaojian, J., Pengpeng, P., & Ke, Z. (2020). Multi-operating mode coordinated control of multi-port energy routers under the framework of energy internet. *Automation of Electric Power Systems, 44*(3), 32–39.
22. Ahmad, J., Tahir, M., & Mazumder, S. K. (2019). Improved dynamic performance and hierarchical energy management of microgrids with energy routing. *IEEE Transactions on Industrial Informatics, 15*(6), 3218–3229.
23. Chen, D., Xu, L., & Yao, L. Z. (2013). DC voltage variation based autonomous control of DC microgrids. *IEEE Transactions on Power Deliverys, 28*(2), 637–648.
24. Chengshan, W. A. N. G., Wei, L. I., & Yifeng, W. A. N. G. (2017). DC bus voltage fluctuation classification and restraint methods review for DC microgrid. *Proceedings of The Chinese Society for Electrical Engineering, 37*(1), 84–98.
25. Novak, H., Lešić, V., & Vašak, M. (2018). Hierarchical model predictive control for coordinated electric railway traction system energy management. *IEEE Transactions on Intelligent Transportation Systems, 20*(7), 2715–2727.
26. Kun, H., Yanman, Li., Xiaoyan, Z., et al. (2021). Research on power control strategy of household-level electric power router based on hybrid energy storage droop control. *Protection and Control of Modern Power Systems, 6*(13), 304–310.
27. Liu, G. Y., Caldognetto, T., & Mattavelli, P. (2017). Power-based droop control in DC microgrids enabling seamless disconnection from upstream grids. *IEEE Transactions on Power Electronics, 34*(3), 2039–2051.
28. Saleh, M., Esa, Y., & Mohamed, A. (2018). Communication based control for DC microgrids. *IEEE Transactions on Smart Grid, 10*(2), 2180–2195.
29. Chunming, T., Meng, Y., & Xiao, F. (2017). An AC-DC hybrid microgrid energy router and operational modal analysis. *Transactions of China Electrotechnical Society, 32*(22), 176–188.
30. Chunming, Tu., Siping, L., Fan, X., & Zheng, L. (2019). Power coordination control strategy of three-port dc energy router based on phase sag. *Power System Technology, 43*(11), 4105–4114.
31. Zhen, L., Wanxing, S., & Qing, D. (2018). Coordinated control strategy of AC/DC hybrid power router based on voltage stabilization by energy storage. *Automation of Electric Power Systems, 43*(2), 121–134.